Gas Phase Reaction Kinetics of Pyruvic Acid with OH-Radicals: The Role of Tunneling, Complex Formation, and Conformational Structure

Jonathan R. Church, Veronica Vaida and Rex T. Skodje*

Department of Chemistry, University of Colorado, Boulder, CO 80309-0215

Abstract

The gas phase reaction of pyruvic acid with the OH-radical is studied theoretically using accurate quantum chemistry and transition state theory. Two chemically distinct H-atom abstraction reactions and two distinct OH addition reactions have been identified. The rate coefficients for these four processes were calculated. Quantum tunneling was included in each rate using the small curvature tunneling method. The influence of the conformational structure of pyruvic acid was found to be particularly intriguing. While the trans-cis structure was found to dominantly react by H-atom abstraction from the methyl site, the trans-trans conformer was found to react mostly through H-atom abstraction from the acid site. A general formalism was developed to model the kinetics of the reactions that involve multiple conformers, interconverting pre-reactive complexes, and multiple transition states. Comparison of the results obtained with available experimental rate observations reveals agreement with the trans-trans conformer of pyruvic acid, but disagreement with the results obtained for a full statistical mixture of reagents. The role of these reactions in the atmospheric processing of pyruvic acid is discussed.

* *Corresponding author:* rex.skodje@colorado.edu

1. Introduction

The importance of hydroxyl radicals (OH) in atmospheric chemistry on Earth has led to concerted efforts to study the OH oxidation of organic molecules and extensive data-bases have been generated over the years.[1 2] These reaction rates are central building blocks for combustion simulations of biofuels and for atmospheric modeling. Nevertheless, multifunctional oxidized

organics with multiple chemically relevant conformations remain a challenge. The rate coefficients for such reactions are often difficult to measure in the laboratory, due to the occurrence of multiple reaction pathways and the rapid proliferation of secondary reactions. Furthermore, there are often stubborn practical issues in generating well characterized gas phase samples. Therefore, one often turns to a theoretical *ab initio* method for the calculation of the rates.[3] Typically, this approach combines a high level determination of the potential energy surface using quantum chemistry coupled with a statistical model for the rate coefficients. These computations can be demanding, due to the size of the molecules involved, and because of our imperfect intuition about the nature of the reaction path itself. Indeed, the mechanistic study of complicated reactions often evolves into global numerical searches for saddlepoints that are quite distinct from our first guess as to the primary reaction site. This failure of imagination can be compounded by a proliferation of non-equivalent conformational structures for the reactants and the transition states (TS) which may lead to very different rates and that require separate optimizations. Furthermore, quantum tunneling and the formation of pre-reactive complexes may modify the rates and are significantly more taxing to model than are direct reactions on the classical barrier. Nevertheless, in principle, a well converged theoretical model will provide a testable prediction for the proposed reaction mechanism and its rate. Thus, theory can provide an avenue to investigate the mechanism of the large organic species that difficult to handle experimentally.

Pyruvic acid ($CH_3(CO)COOH$) provides an informative molecular system whose reactivity exemplifies the complexity inherent in organic molecules relevant on Earth. It is one of the most abundant keto-acids found in the troposphere[4 5 6 7 8 9 10] and is formed as an intermediate species in the isoprene oxidation pathway.[4] Pyruvic acid itself has been found in the troposphere in different types of climates such as mid-latitude, tropical and marine environments with large gas phase mixing ratios up to 100 ppt.[6 7 8 9] It has also been found in several different media, including the gas phase, rainwater, aerosols, and snow.[11 12 13 14 15 16 17] Experimental studies on the reactivity of this molecule have suggested that direct photolysis is the primary pathway for degradation in the troposphere rather than that of OH oxidation.[18 19 20 21 22 23] The oxidation of pyruvic acid by OH remains of interest however and given the sparsity of information available on a system of this complexity, theory can provide an avenue to investigate the mechanism of organic species difficult to handle experimentally.

In this work, we provide a theoretical study of the gas phase reaction rate of pyruvic acid with OH radicals yielding the rate coefficients and mechanism. In addition to its practical significance for chemistry of the atmosphere, this work also provides an interesting study of the influence of complexities such as multi-structural effects, pre-reactive complex formation, and substantial tunneling on the reaction rate. We have computed the rate coefficients for the elementary reaction steps using *ab initio* transition state theory,[24] i.e. transition state theory (TST) in which all the required frequencies and structures are obtained from quantum chemistry calculations. These elementary rates are combined in a kinetic model to produce an effective rate coefficient. The pressure dependence was considered but found to be of negligible importance. There are two nascent product channels of importance that differ by the abstraction site, i.e.

$CH_3(CO)COO\mathbf{H}+OH \rightarrow CH_3CO+CO_2+H_2O$ (Acid site-abstraction)

$C\mathbf{H}_3(CO)COOH+OH \rightarrow CH_2(CO)COOH+H_2O$ (Methyl site-abstraction)

We also find two addition reactions which turn out to be of lesser kinetic importance due to their higher barriers

$CH_3(CO)COOH+OH \rightarrow CH_3COCO(OH)_2$ (Acid site addition)

$CH_3(CO)COOH+OH \rightarrow CH_3CO(OH)COOH$ (Ketone site addition)

The PA molecule possesses four stable conformational structures that are shown in Fig. 1. The lowest energy conformer, the trans-cis (Tc) species, is stabilized by hydrogen bonding between the acidic H-atom and the ketonic oxygen. The trans-trans (Tt) species differs by the orientation of the hydroxyl H-atom which now points toward the ketone group. There are two other structures, the cis-trans (Ct) and cis-cis (Cc) conformers, which are even higher in energy and play little role in the kinetics except at high temperatures. Based on a theoretical determination of the free energies (discussed in Sec. 2), the relative equilibrium concentrations these species in a 298K dilute gas will be 0.98 (Tc) and 0.02 (Tt). We have noted previously[25] [26] that these conformers exhibit very different vibrational spectra due to the H-atom chattering between the oxygen atoms at high overtone excitation. We anticipate that the reaction kinetics will also show a significant conformational effect, since the acidic H-atom is a primary site for reactions with OH-radicals. The potential influence of multiple conformers on reaction kinetics has been appreciated for many years. In organic synthesis, e.g., the well-known Curtin-Hammett principle[27] was developed in

the 1950's in an attempt to correlate the product distribution of a reaction to the propensity of conformal isomers of the reagent. More recently, transition state theory has been extended to incorporate the influence of distinct transition state structures on the overall rate of reaction.[28] [29] [30]

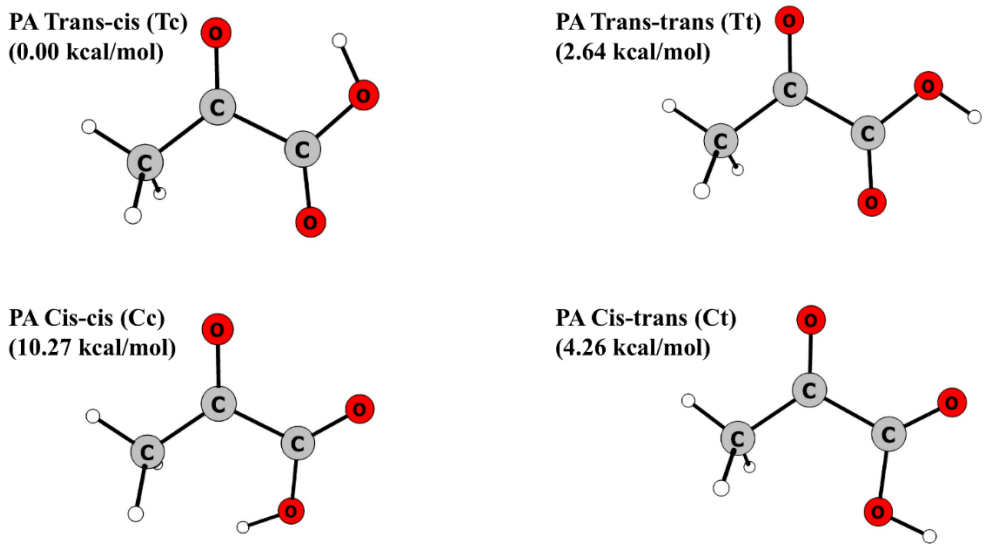

Figure 1. *The four conformational structures of the pyruvic acid molecule. The energies are the harmonic zero point corrected relative energies computed using quantum chemistry at the level CCSD(T)/CBS//M11/cc-pVTZ.*

The role of hydrogen bonded intermediates in bimolecular reactions of organic molecules with OH have been discussed.[31] [32] [33] It is well known that many organic species will exhibit significant trapping potential wells with OH-radicals due to hydrogen bonding or van der Waals interactions.[34] The formation of such pre-reactive complexes (PRC's) can yield highly curved Arrhenius plots and can even lead to apparent negative activation energies, in particular when the reaction barrier is submerged below the entrance channel threshold. These effects have been described extensively in the literature[35] [36] [37] [38] [39] [40] [41] with Mozurkewich and Benson[42] producing a general statistical theory for negative activation energies. The pre-reactive complexes, like the reactants and the TS's, possess different conformational structures, which may correlate different transition states via distinct reaction pathways. This occurs for PA+OH and adds an additional layer of complexity to the rate modeling.

The remainder of this paper is organized as follows. In Sec. 2, the quantum chemical methods and results are presented. The molecular structures are computed using DFT and the energies of the stationary points, i.e. the reactants, products, transition states, and intermediate

complexes were determined using a coupled cluster complete basis set method. The minimum energy pathways were mapped out for a number of the saddlepoints to determine the mechanisms and to compute tunneling corrections. In Sec. 3, the kinetics of the OH+PA is discussed. A generalized steady state approximation is introduced to compute the effective reaction rate. In Sec. 4 the TST formulae used are presented, while the supporting information describes the adaptation of the formalism to microcanonical ensembles. The quantum tunneling is incorporated by the small curvature tunneling approximation.[43] [44] Section 5 presents a discussion of the computed rate expressions and comparison with available experimental results. Section 6 is a conclusion that suggests possible future work and speculation about the certain discrepancies with previous works.

2. Quantum Chemistry: Structures and Energetics

The optimized structures for reactants, products and saddlepoints were obtained by DFT using the Minnesota functional M11[45] and the cc-pVTZ basis set. This functional has been shown to perform well for a number of related radical reactions.[46] The M11/cc-pVTZ calculations were performed using the GAMESS-US software package[47]. The vibrational normal mode frequencies for each structure were obtained at the same level of theory as the geometry optimizations. Consistent with convention, we scale the frequencies by a factor 0.967.[48] The intrinsic reaction coordinate, *s*, was calculated starting from the saddle point using the M11/cc-pVTZ level of theory with the Gonzalez-Schlegel 2nd order (GS2) path following algorithm.[49] The energy for each stationary point was determined using ROCCSD(T) and by extrapolation to the complete basis set (CBS) limit using cc-pVnZ (n=D, T, Q) basis sets. These calculations were performed using the Gaussian 16 software package [50]. The zero point and CBS limit energies were used to calculate the harmonic zero-point corrected (i.e. adiabatic) barriers as well as the reaction energy for each reaction, and the results are presented in Table 1. Also shown in Table 1 are some of the results obtained using the lower level M11/CBS determination of the energies. For the TS-barriers, the results of the CCSD(T) calculations are generally lower than those for M11, sometimes substantially so. Additionally, we have located several saddlepoints between conformers of the PRC's and the reagents, the energetics for those barriers are given in Table 2.

Table 1. The harmonic zero-point corrected energies (kcal/mol) for the PA+OH reaction where the threshold energy for PA_{Tc}+OH is set to zero. The odd numbered reactions

originate from the PA_{Tc} conformer while the even numbered reactions originate from the PA_{Tt} conformer. The results are at the CCSD(T)/CBS//M11/cc-pVTZ level while the numbers in parentheses are computed using M11/CBS//M11/cc-pVTZ. The ΔH_{rxn} for the starred reactions are to post reactive complexes.

	$PA + OH$	ΔE_{PRC}	ΔE_{TS}	ΔH_{rxn}
R1 (Methyl Abstraction, Tc)	0.00 (0.00)	-3.04 (-2.23)	4.27 (4.71)	-23.11 (-24.37)
R2 (Methyl Abstraction, Tt)	2.64 (2.87)	-0.87 (-0.21)	6.24 (6.91)	-20.43 (-21.26)
R3 (Acid Abstraction, Tc)	0.00 (0.00)	-3.44 (-4.52)	6.97 (5.11)	-36.14 (-40.26)
R4 (Acid Abstraction, Tt)	2.64 (2.87)	-3.01 (-3.79)	4.64 (5.93)	-36.14 (-40.26)
R5 (Acid Addition, Tc)	0.00 (0.00)	-	7.01 (11.04)	-5.29 (-3.24)*
R6 (Acid Addition, Tt)	2.64 (2.87)	-	11.79 (13.07)	-29.78 (-32.96)
R7 (Ketone Addition, Tc)	0.00 (2.87)	-	5.75 (10.14)	-27.89 (-30.46)
R8 (Ketone Addition, Tt)	2.64 (2.87)	-	6.29 (10.63)	-16.17 (-15.14)*

Table 2. Isomerization energetics in kcal/mol. The results were computed at the CCSD(T)/CBS//M11/cc-pVTZ level while the numbers in parentheses are computed using M11/cc-pVTZ //M11/CBS.

	ΔE_{TS}	ΔH_{rxn}
PA(Tc→Tt)	12.42 (12.48)	2.64 (2.87)
PA(Tc→Ct)	-	4.26 (4.58)
PA(Tc→Cc)	-	10.27 (10.68)
PRC1→PRC3	3.04 (2.23)	-0.40(-2.29)
PRC2→PRC4	3.51 (3.08)	-2.14(-3.58)
PRC3→PRC4	5.39 (5.52)	0.43 (0.73)

The Tc conformer is lower in energy than the Tt conformer by 2.64 kcal/mol at the CCSD(T)/CBS level. The energy difference is primarily due to intramolecular hydrogen bonding between the hydrogen atom of the hydroxyl group and ketonic oxygen atom that occurs only for the Tc conformer. The theoretical splitting of 2.64 kcal/mol is somewhat larger than that inferred from experiment, i.e. Reva *et al.* reported a value of 2.08 (±0.31) kcal/mol[51] while Schellenberger *et al.* obtained 2.34 (±0.32) kcal/mol.[52] These results provide calibration of the accuracy of the present QM calculations. We note that the isomerization of the Tc and Tt forms of PA is hindered by a high barrier of 12.42 kcal/mol that separates the two conformers as shown in Table 2.

We have identified and characterized the eight energetically lowest saddlepoints for the PA+OH reaction which correspond to eight distinct reaction pathways. The optimized transition

state structures are shown in Fig. 2. The TS's can be classified by the conformational structure and the reaction type, i.e. there are two important TS conformers per type of reaction, the Tt and Tc. The reaction pathways and TS's are labeled as R1-R8, and TS1-TS8, respectively. Here, R1 and R2 are abstraction reactions of a methyl H-atom of the Tc and Tt conformer of PA, respectively. Likewise, R3 and R4 are abstraction reactions of the acidic H-atom from Tc and Tt conformers. The two addition reactions are similarly paired with Tc and Tt for R5-R8 and TS5-TS8. Following the reaction pathways forward from the TS, we find that the reaction R_n naturally correlates with the following product distributions P_n given by

P1: $CH_2(CO)COOH(Tc)+H_2O$

P2: $CH_2(CO)COOH(Tt)+H_2O$

P3: $CH_3CO+CO_2+H_2O$

P4: $CH_3CO+CO_2+H_2O$

P5: $CO(OH)_2+CH_3CO$

P6: $CO(OH)_2+CH_3CO$

P7: $COOH+CH_3COOH$

P8: $COOH+CH_3COOH$

We have found the existence of hydrogen bonded post-reactive complexes for reactions R5 and R7. For the R5 reaction which correlates to the reagent PA_{Tc}+OH, a complex is produced due to the hydrogen bonding between the acid and carbonyl functional groups. For the PA_{Tt}+OH correlated R6 reaction, on other hand, the reaction path in the exit channel shows no complex well and the products fall apart directly to carbonic acid and an acetyl radical. Likewise, for the addition reaction to the ketone carbon, the PA_{Tc}+OH R7 process yields $COOH+CH_3COOH$ directly while R8 yields a complex weakly bound by hydrogen bonding.

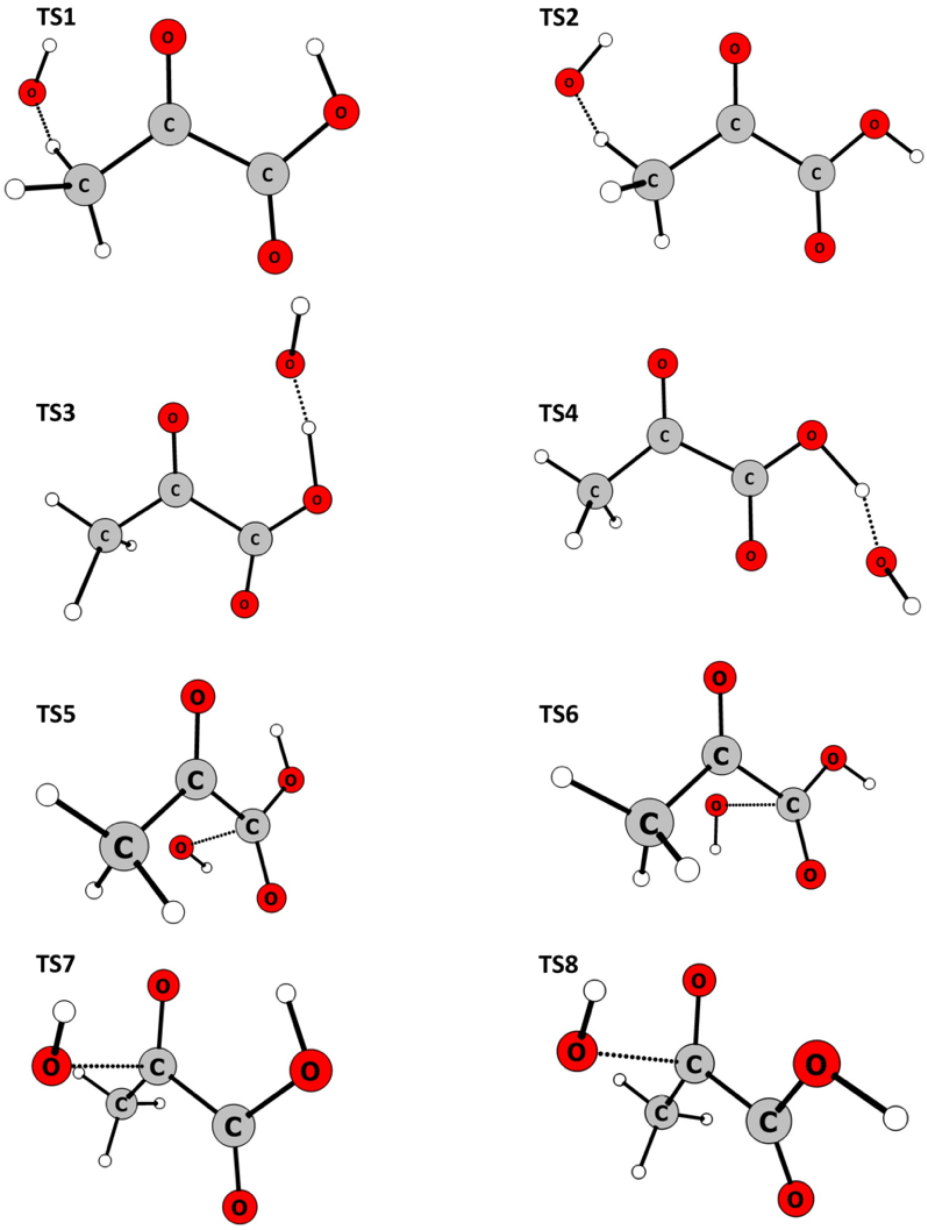

Figure 2. *Transition state structures obtained using M11/cc-pVTZ for the OH+PA reactions. TS1, TS3, TS5, and TS7 originate from the trans-cis conformer of pyruvic acid and TS2, TS4, TS6, and TS8 originate from the trans-trans conformer of pyruvic acid.*

The reaction pathways for R1-R4 were found to exhibit clear pre-reactive complex wells. Those structures were obtained at the M11/cc-pVTZ level and are shown in Fig. 4.

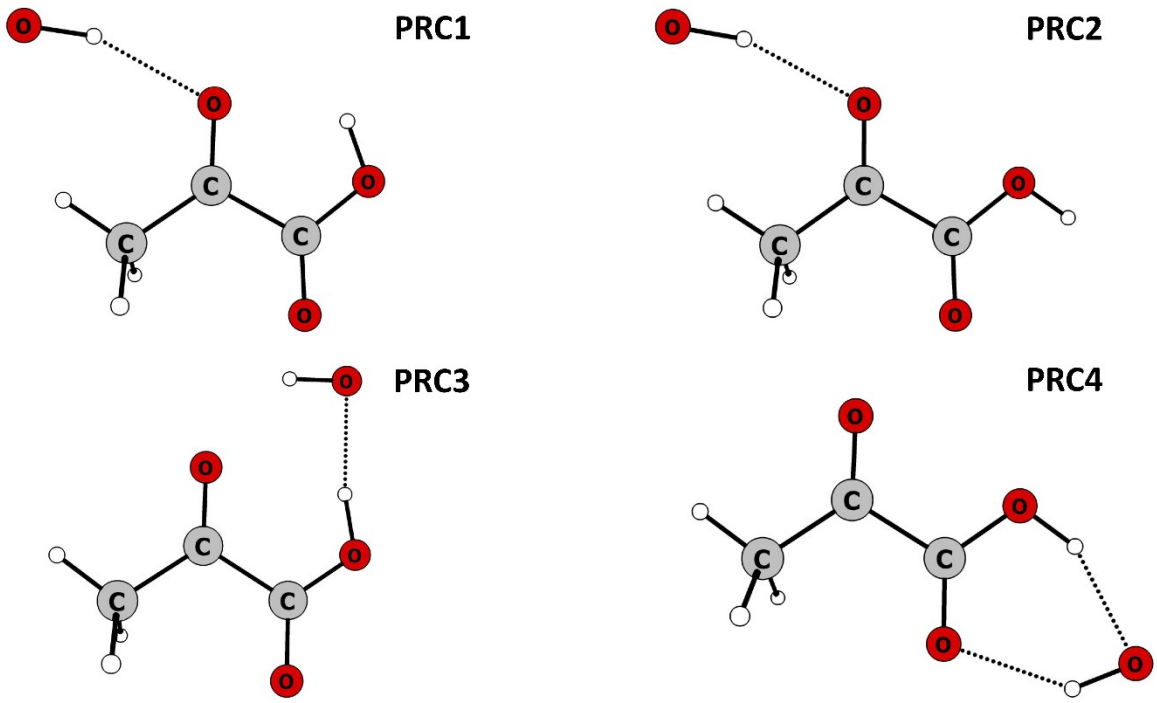

Figure 3. *Pre-reactive complex structures obtained using M11/cc-pVTZ for the OH+PA reactions. PRC1 and PRC3 originate from the trans-cis conformer of pyruvic acid and PRC2 and PRC4 originate from the trans-trans conformer of pyruvic acid.*

The pre-reactive complexes, PRC1 and PRC2, show a hydrogen bond forming between the H-atom of the attacking OH-radical and the carbonyl O-atom. These two PRC's clearly correspond to the Tc and Tt forms of the reagent PA molecule. Comparison to the structures shown in Fig. 2 for the transition states suggests that an H-atom abstraction reaction from the methyl group can easily occur between PRC1 and TS1 and between PRC2 and TS2. For the complexes PRC3 and PRC4, the hydroxyl radical forms a planar ring type structure between the carboxylic acid H-atom and a carbonyl O-atom. In the PRC3 complex the OH radical is hydrogen bonding to the ketonic oxygen and the acid OH. On the other hand, in the PRC4 complex the OH radical shows hydrogen bonding only within the acid functional group. These complexes correlate to TS3 and TS4.

The chemical energetics that is presented in Table 1 can be used to anticipate reaction pathways that may contribute to the overall PA+OH kinetics. Pursuant to this, the relevant energies for the reactions R1-R8 are organized graphically in Figs. 4 and 5. In Fig. 4, the OH+PA_{Tc} reagent is joined to the pre-reactive complexes, transition states, and products of similar conformational structure, i.e. TS1, TS3, TS5, TS7 and PRC1, PRC3, respectively. In Fig. 6 the

OH+PA_{Tt} reagent is likewise joined with the structurally similar TS2, TS4, TS6, TS8 and PRC2, PRC4. The lowest adiabatic reaction barrier for PA_{Tc}+OH for the methyl H-atom abstraction, i.e. TS1, lies 4.27 kcal/mol above the entrance asymptote. The acid abstraction reaction barrier lies considerable higher, 6.97 kcal/mol. The addition reactions also occur with higher barriers of 7.02 and 5.75 kcal/mol for R5 and R7, respectively. The reactions of OH+PA_{Tt}, depicted in Fig. 5, which are offset in energy by 2.64 kcal/mol from the absolute scale in Table 1, reveal that the acid site H-atom abstraction reaction has the lowest adiabatic barrier of 1.99 kcal/mol (TS4) while the methyl site abstraction (TS2) lies somewhat higher at 3.04 kcal/mol. The addition reactions yield higher barriers of 11.79 and 6.29 kcal/mol for TS6 and TS8. The transition state energies predicted by CCSD(T) calculations are generally lower than those of M11. The addition reactions, in particular, are significantly lower. The pre-reactive complexes, PRC3 and PRC4 were found to have deeper wells than those for PRC1 and PRC2. The increased well depths can be ascribed to the greater stabilizing effect of ring formation with the acid functional group. The complexes PRC1 and PRC2 have very similar well depths, which is understandable due to the similarity between the two structures. The pre-reactive complexes PRC3 and PRC4, on the other hand, were found to have relatively large energetic differences. The distinct ring structure for PRC4 in the R4 reaction clearly has greater stabilizing effect than that for the PRC3 complex with CCSD(T)/CBS predicting a difference of 2.22 kcal/mol.

The reaction energetics suggests an interesting potential distinction between reactivity of the PA_{Tc} and PA_{Tt} conformers. Specifically, Tc conformer favors the methyl site H-abstraction reaction while the Tt conformer favors the acid site H-abstraction reaction. In full treatment of the reaction kinetics, however, we must bear in mind that the entropy of activation, tunneling correction, and relative thermal PA_{Tc}/PA_{Tt} abundances must also be considered. Furthermore, the reactions that proceed through pre-reactive complex formation may favor the acid site abstraction since those wells are deeper. In the next section we shall explore these effects using a statistical model for the reaction.

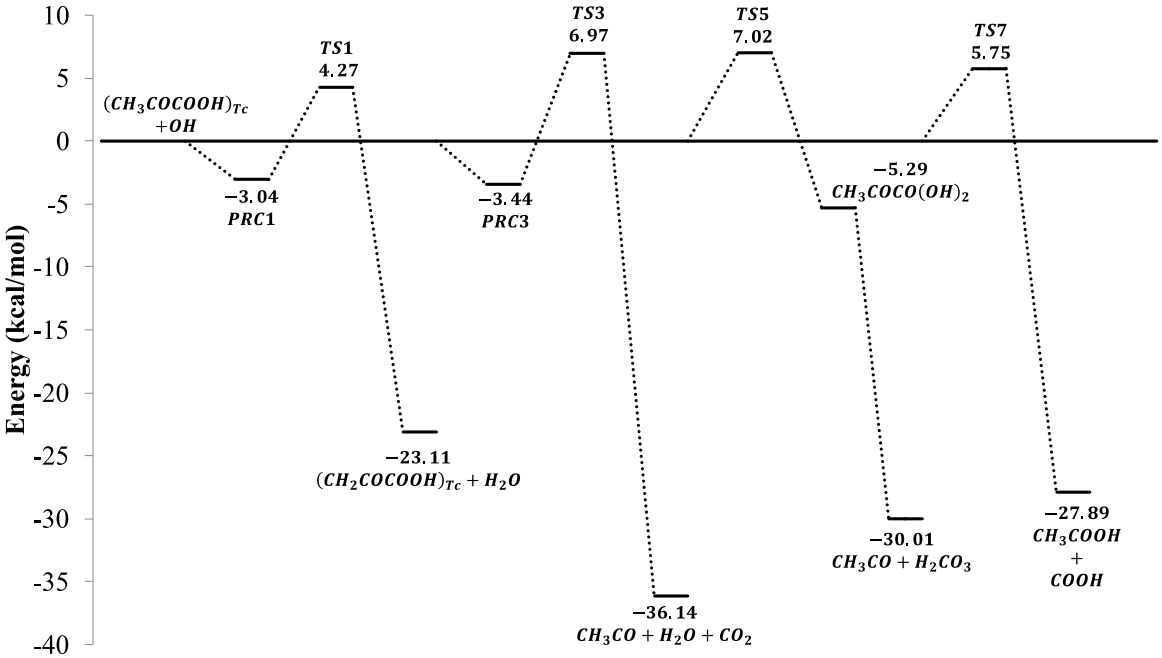

Figure 4. *The harmonic zero point energies of the stationary points that most +closely correlate with the reaction of the Tc conformer of pyruvic acid with an OH radical. The results were computed using the CCSD(T)/CBS//M11/cc-pVTZ method. The pre-reactive complexes for reactions R1 and R3 are indicate as is the post-reactive complex for R5.*

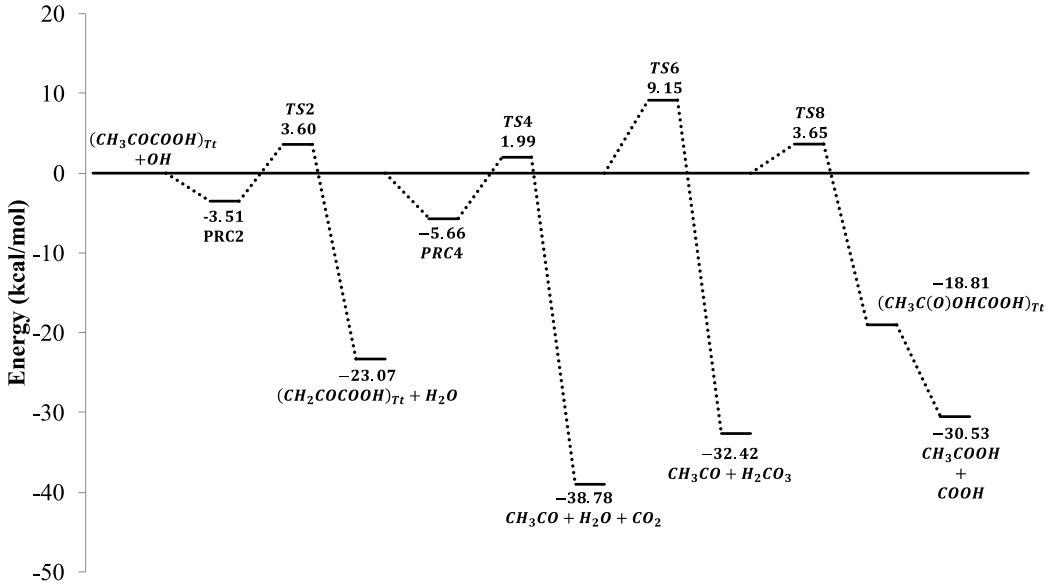

Figure 5. *The harmonic zero point energies of the stationary points that most closely correlate with the reaction of the Tt conformer of pyruvic acid with an OH radical. The results were computed using the CCSD(T)/CBS//M11/cc-pVTZ method. The pre-reactive complexes for reactions R2 and R4 are indicate as is the post-reactive complex for R8.*

3. Kinetic Model

The goal of the present work is to determine the phenomenological rate coefficient k_{eff} for disappearance of PA, i.e.

$$\frac{d[PA]}{dt} = -k_{eff}[PA][OH] \tag{3.1}$$

where

$$[PA] = [PA_{Tt}] + [PA_{Tc}] \tag{3.2}$$

We shall assume that $[PA_{Tt}]$ and $[PA_{Tc}]$ always lie in thermal equilibrium. The temperature and pressure are taken to be comparable with atmospheric values. The expression for k_{eff} may vary depending on whether we adopt the canonical or microcanonical formulation of the rate, how the PRC's interconvert, and how the magnitudes of the decay rates of the PRC's in the forward and reverse directions compare with one another. In principle there are eight distinct reactions that may contribute, R1-R8, however we will simplify the discussion from the start by noting the rates for the addition reactions are negligible under our conditions so only the four abstraction reactions R1-R4 contribute to the effective rate constant.

The abstraction reaction of PA with OH can be viewed as either a direct abstraction process or an indirect complex forming process. In the latter scheme, the reaction occurs by first forming a PRC, occurring with a loose transition state, which then can react to form products over a tight transition state or return to reactants. For the case of a single conformational structure, it is well known that these scenarios lead to two potential forms of the reaction rate R,

$$PA + OH \underset{k_d}{\rightarrow} Product \qquad R = k_d[PA]\,[OH] \tag{3.3}$$

and

$$PA + OH \underset{k_{\pm f}}{\leftrightarrow} PRC \underset{k_r}{\rightarrow} Product \qquad R = \frac{k_f k_r}{k_{-f} + k_r}[PA][OH] \tag{3.4}$$

where the latter rate is obtained assuming a steady state value for the concentration of the intermediate

$$[PRC] \approx \frac{k_f}{k_{-f} + k_r}[PA][OH] \tag{3.5}$$

The indirect mechanism reduces to the direct mechanism form when the backward breakup rate (k_{-f}) is much larger than the forward rate (k_r), i.e

$$k_{eff} = \frac{k_f k_r}{k_{-f}+k_r} \approx \frac{k_r k_f}{k_{-f}} = k_r K_{eq} \qquad (3.6)$$

Similar expressions can be written in the microcanonical formalism that is appropriate for cases where E and J are conserved and are presented in the supporting information.[38 39 40 42] Assuming a single TS and employing the usual TST expression, k_{eff} obtained in this fashion is identical to the expression obtained for direct bimolecular reaction, k_d. Hence, we adopt the indirect mechanism as the general mechanism and regard direct reaction as a special limiting case valid for $k_{-f} >> k_r$.

Multiconformational TST has been discussed previously although, here, we formulate the problem in a somewhat different way to obtain an expression for k_{eff} that incorporates all reactions and PRC's within the SSA. The basis of our model is the following physical picture. A given reactant conformer (Tt or Tc) of PA will combine with OH to form an intermediate of similar structure to the reactant. This is reasonable since the barrier to conformational isomerization of free PA is high, i.e. 12.4 kcal/mol (see Table 2). Thus, OH+PA_{Tc}→PRC1 (or PRC3) and OH+PA_{Tt}→PRC2 (or PRC4). These processes are modeled as rapid barrierless association reactions. The pre-reactive complexes can have several possible fates. They may return to reagents over a loose TS, react over the tight TS with similar structure, or they may isomerize among themselves. The latter possibility is considered since we have found that some of the isomerization barriers of the PRC's are much lower than those of the "free" PA. We distinguish between two possible classes of isomerization: conformational isomerization, e.g. PRC1→PRC2 or PRC3→PRC4, and roaming isomerization, PRC1→PRC3 or PRC2→PRC4. In the latter case, the abstraction site itself changes when the OH-radical migrates. Since we distinguish between conformers at every stage of process, the rate coefficients must be indexed to label the initial and final species of each elementary reaction. As depicted in Fig. 6, the formation rates coefficients $k_f^{j,i}$ are organized as a 2×4 matrix

$$PA_i \rightarrow PRC_j, \;\; rate = k_f^{i,j}\,[PA_i] \qquad (3.7)$$

In our convention, PA_1=PA_{Tc}, PA_2=PA_{Tt}, and the PRC_j are defined consistent with numbering scheme in Fig. 3. As we noted above, $k_f^{i,j} = 0$ when (i,j)=(1,2), (1,4), (2,1), and (2,3) since the

model requires the conformation structure to be preserved during complex formation. The breakup rate coefficients are found from micro-reversibility

$$k_{-f}^{i,j} = K_{eq}^{i,j} k_f^{i,j} \quad with \quad K_{eq}^{i,j} = \frac{Q_{PRC_j}}{Q_{PA_i} Q_{OH}} \cdot e^{-\frac{\Delta E_{i,j}^0(c)}{k_B T}} \tag{3.8}$$

where $\Delta E_{i,j}^0(c)$ is the zero point energy difference between PA_i+OH and PRC_j, while Q_{PRCj}, Q_{PAi}, and Q_{OH} are the canonical partition functions per unit volume for the indicated species, including electronic. In order to achieve notational consistency, in eq. (3.8) we set $PA_i=PA_{Tc}$ for i=1,3 and $PA_i=PA_{Tt}$ for i=2,4. Hence, $k_f^{1,j} = k_f^{3,j}$ *and* $k_f^{2,j} = k_f^{4,j}$. The reaction rates for PRC_j→products are represented as a diagonal 4×4 matrix $k_r^{i,j}$. The isomerization rate constants, $k_{iso}^{i,j}$ and $k_{roaming}^{i,j}$, are sparse 4×4 matrices for PRC_j→PRC_i. The $k_{iso}^{i,j}$ is only non-zero for (i,j)=(1,2)=(2,1) and (i,j)=(3,4)=(4,3), which are conformational changes on the same site. The roaming type isomerizations $k_{roaming}^{i,j}$ are non-zero only for like conformers between different binding sites, i.e. (i,j)=(1,3)=(3,1) and (i,j)=(2,4)=(4,2). A schematic of the reaction mechanism and the obvious rate equations are shown in Fig. 6. The matrix $K_I^{i,j}$ in the equations is the net isomerization rate between PRC_i and PRC_j, i.e. $K_I^{i,j} = \delta_{i,j} \sum_i \left(k_{iso}^{i,j} + k_{roaming}^{i,j}\right) - \left(k_{iso}^{j,i} + k_{roaming}^{j,i}\right)$. The $k_{iso}^{i,j}$ *and* $k_{roaming}^{i,j}$ satisfy reversibility as does $K_I^{i,j}$.

As diagrammed in Fig. 6, a steady state approximation for the "vector" of **PRC** concentrations $[\mathbf{PRC}]_{ss}$ can be obtained in matrix analogy to eq. (3.5)

$$[\boldsymbol{PRC}]_{ss} = \left[\boldsymbol{k}_{-f} + \boldsymbol{K}_I + \boldsymbol{k}_r\right]^{-1} \cdot \boldsymbol{k}_f \cdot [OH][\boldsymbol{PA}] \tag{3.9}$$

The 4×4 inverse matrix $\left[\boldsymbol{k}_{-f} + \boldsymbol{K}_I + \boldsymbol{k}_r\right]^{-1}$ is diagonal only when $\boldsymbol{K_I}$ is zero. If the PA conformers lie in an equilibrium distribution with weights p_1 (Tc) and p_2 (Tt) where $p_1+p_2=1$, then the effective rate of PA reaction is

$$Rate = \; Tr\left(\boldsymbol{k}_r \cdot \left[\boldsymbol{k}_{-f} + \boldsymbol{K}_I + \boldsymbol{k}_r\right]^{-1} \cdot \boldsymbol{k}_f \cdot \boldsymbol{\Lambda}_B\right)[OH][PA] = \; k_{eff}[OH][PA] \tag{3.10}$$

where we define $\boldsymbol{\Lambda_B} = \delta_{ij} p_i$ as the diagonal matrix of equilibrium statistical weights for the PA conformers with $[\mathbf{PA}] = \boldsymbol{\Lambda_B}[PA]$. For notational consistency, we add the redundant definitions

p_3=p_1 and p_4=p_2. If in eq. (3.9), the $\mathbf{k}_{-f}$ term dominates over $\mathbf{K}_I$ and $\mathbf{k}_r$ then we obtain the equilibrium approximation

$$[\boldsymbol{PRC}]_{eq} \approx \boldsymbol{K}_{eq} \cdot \boldsymbol{\Lambda}_B [OH][PA] \tag{3.11}$$

then

$$k_{eff} = Tr\big(\boldsymbol{k}_r \cdot \boldsymbol{K}_{eq} \cdot \boldsymbol{\Lambda}_B \big) \tag{3.12}$$

In this scenario, the relative concentrations of the PRC's form an equilibrium distribution with the PA+OH reagents, i.e.

$$\frac{[PRC_i]}{[PRC_j]} = \frac{p_i}{p_j} \frac{Q_{PRCi}}{Q_{PRCj}} e^{-\frac{\Delta E^0_{i,j}(c)}{k_B T}} \tag{3.13}$$

where i and j$\in$(1-4). The limit described by eq. (3.12) assumes the reverse reaction ($\mathbf{k}_{-f}$) dominates the PRC kinetics and the computation of $k_{eff}(T)$ becomes straightforward as the rates for each reaction R1-R8 can be calculated independently and summed. The net reaction rate is then the thermally weighted average,

$$k_{eff}(T) = \sum_{i=1}^{8} p_i k_i \approx \sum_{i=1}^{4} p_i k_i \tag{3.14}$$

where the approximate sum reflects the negligible contribution of the addition reactions and $k_i = \big(\boldsymbol{k}_r \cdot \boldsymbol{K}_{eq} \big)_{i,i} = k_r^{i,i} K_{eq}^{i,i}$. These k_i's are simply the direct reaction rate coefficients for the elementary processes PA_i+OH→TS_i→$Product_i$.

On the other hand, it is clear that if the reverse rates, $\mathbf{k}_{-f}$, do not dominate in $\big[\boldsymbol{k}_{-f} + \boldsymbol{K}_I + \boldsymbol{k}_r\big]^{-1}$ then deviations from the simple form eq. (3.14) are possible in some cases. Consider the following scenarios. When the PRC interconversion rates, $\mathbf{K}_I$ are large or comparable to $\mathbf{k}_{-f}$, but yet $\mathbf{k}_r$ remains small, then the assumption of micro-reversibility for $K_I^{i,j}$ guarantees that the PRC concentrations remain in overall equilibrium with the reagents and hence eq.(3.14) is still useful. Conversely, if the isomerization rates $\mathbf{K}_I$ are small but the forward rates $\mathbf{k}_r$ are large, then eq. (3.14) is replaced by the generalized steady state expression but the reactions are still independent

$$k_{eff} = \sum_{i=1}^{4} p_i \cdot \frac{k_f^{i,i} k_r^{i,i}}{k_{-f}^{i,i} + k_r^{i,i}} \qquad (3.15)$$

Finally, if rates $\mathbf{K}_I$ and $\mathbf{k}_r$ are both large with respect to $\mathbf{k}_{-f}$, then the PRC's can interconvert and the effective rate is no longer the weighted sum of independent rate expressions but becomes coupled. Our calculations imply eq. (3.14) is appropriate for the present case.

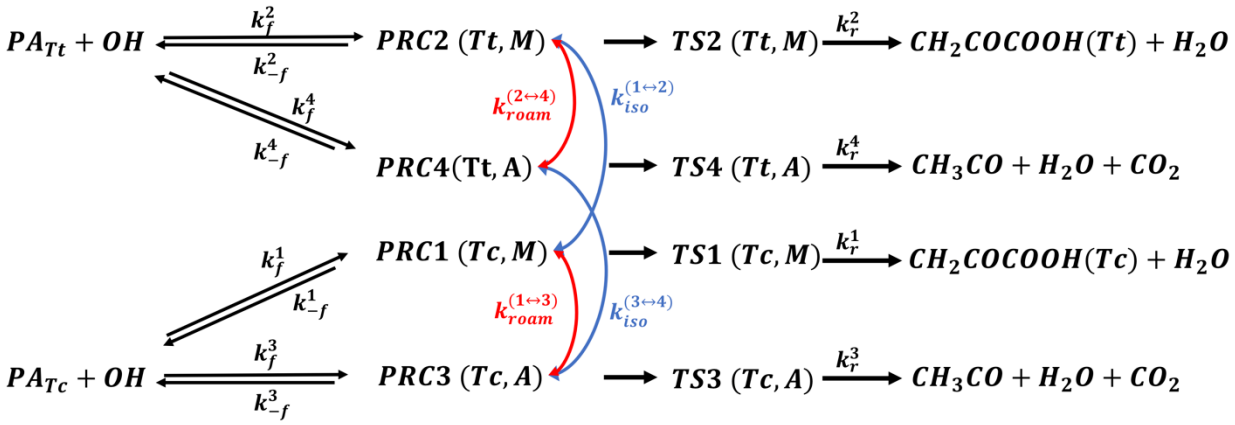

$$\frac{d\overrightarrow{[PA]}[OH]}{dt} = -\overline{\overrightarrow{k_f}} \cdot \overrightarrow{[PA]}[OH] + \overline{\overrightarrow{k_{-f}}} \cdot \overrightarrow{[PRC]}$$

$$\frac{d\overrightarrow{[PRC]}}{dt} = \overline{\overrightarrow{k_f}} \cdot \overrightarrow{[PA]}[OH] - \left(\overline{\overrightarrow{k_{-f}}} + \overline{\overrightarrow{k_r}} + \overline{\overrightarrow{K_I}}\right) \cdot \overrightarrow{[PRC]}$$

$$\frac{d\overrightarrow{[Prod]}}{dt} = \overline{\overrightarrow{k_r}} \cdot \overrightarrow{[PRC]}$$

Figure 6. *A schematic diagram showing the reaction mechanism involving two conformers of PA, four PRC's, and four reactive transition states. The kinetic equations in matrix form is also indicated.*

4. Transition State Theory Computations

The elementary rate coefficients for single steps were explicitly computed using transition state theory (TST) assuming a harmonic oscillator-rigid rotor model for the reagents and transition states based on stationary point single geometries. Each conformer and TS were taken as independent consistent with the harmonic approximation to the torsional modes. To model the direct reaction of PA through a TS "β" the TST expression is

$$k_d^{\beta}(T) = \kappa_{\beta}\eta_{\beta}\frac{k_B T}{h}\frac{Q_{\beta}^{\ddagger}}{Q_{OH}Q_{PA(\beta)}}e^{-\frac{\Delta E_{\beta}^{\ddagger}(d)}{k_B T}} \qquad (4.1)$$

In the present scheme, a given TS "β" is paired with the structurally similar PA conformer, PA(β), and so $\Delta E_{\beta}^{\ddagger}(d)$ is taken as the zero-point corrected barrier between the β transition state and the reagent pair of PA(β)+OH. In this scheme, we have PA(β)= PA_{Tc} when β=1,3 and PA_{Tt} when β=2,4. The κ_β is the quantum transmission coefficient for the TS_β which is computed using the SCT method.[43 44] We note that each methyl abstraction reaction has a reaction path degeneracy of three and every transition state structure studied for the OH reactions had a non-superimposable mirror image. These numerical factors then multiply the rate coefficients as η_β. The electronic contribution to Q_{OH} is explicitly included. The canonical unimolecular rate coefficients at temperature T for reaction of PRC_i across TS_i is given by (since here $k_r^{i,j}(T) = 0$ if i≠j)

$$k_r^{i,i}(T) = \kappa_i \eta_i \frac{k_B T}{h} \frac{Q_i^{\ddagger}}{Q_{PRC}^{i}} e^{-\frac{\Delta E_{i,i}^{\ddagger}(c)}{k_B T}} \tag{4.2}$$

where $\Delta E_{i,i}^{\ddagger}(c)$ is the zero-point corrected barrier between PRC_i and TS_i. Thus, $\Delta E_{i,i}^{\ddagger}(c)$ is larger than $\Delta E_{i}^{\ddagger}(d)$ by the zero-point corrected well depth of PRC_i, $\Delta E_{i,i}^{0}(c)$. The reverse reaction occurs across a loose transition state,

$$k_{-f}^{i,i}(T) = \frac{k_B T}{h} \frac{Q_{L,i}^{\ddagger}}{Q_{PRC}^{i}} e^{-\frac{\Delta E_{i,i}^{0}(c)}{k_B T}} \tag{4.3}$$

The barrierless complex formation rates are, consistent with reversibility eq. (3.8), given by

$$k_f^{i,i}(T) = \frac{k_B T}{h} \frac{Q_{L,i}^{\ddagger}}{Q_{OH} Q_{PA(i)}} \tag{4.4}$$

In analogy to eq. (4.2) the conformational isomerization coefficients $k_{iso}^{i,j}(T)$ are

$$k_{iso}^{i,j}(T) = \kappa_i \eta_i \frac{k_B T}{h} \frac{Q_{i,j}^{\ddagger,\mathrm{iso}}}{Q_{PRC}^{i}} e^{-\frac{\Delta E_{i,i}^{\ddagger,iso}(c)}{k_B T}} \tag{4.5}$$

The $Q_{L,i}^{\ddagger}$ expressions can be approximated by the free rotor approximation. The roaming rates coefficients $k_{roaming}^{i,j}(T)$ are less well understood and may need to be similarly approximated. Using approximate RRK-expressions developed by Truhlar and co-workers,[53] we have found that $k_{-f}^{i,i}(T)$ are orders of magnitude larger than $k_r^{i,i}(T)$ which suggests that eq. (3.14) is likely

sufficient for the PA+OH application. Pressure effects were estimated using the master equation approach and were found to be very small in the present case.[54]

V. Results

In Table 3 we show the values of k_i for i=1-8 calculated for several values of temperature. Also listed are the thermally weighted values, $p_i k_i$, and the tunneling coefficients κ_i. It is seen that the addition reactions R5-R8 are smaller by over two orders of magnitude compared to the abstraction reactions R1-R4. Indeed, it is found that reactions R5-R8 have a negligible impact on the overall rate regardless of the modeling scenario chosen. Some significant differences are observed between the various abstraction reactions. The H-abstraction from the acid group (R3 and R4) occurs with lower barriers than abstraction from the methyl group, R1 and R2. However, the conformational ordering is reversed between the two abstraction sites, i.e $\Delta E_{TS}(R3) > \Delta E_{TS}(R1)$ while $\Delta E_{TS}(R2) > \Delta E_{TS}(R4)$. The tunneling coefficients favor the acid abstraction since the reaction barriers are narrower, as shown in parentheses in Table 3. In Fig. 7 we show the rate coefficients for R1-R4 plotted as functions of temperature. We note that the rate coefficient for the acid abstraction reaction from the Tt conformer, i.e. R4, shows a clear negative temperature dependence while the other processes display a positive activation energy albeit with very curved Arrhenius plots. Before the application of thermal weighting factors to the rate coefficients we observe the PA_{Tt}+OH reactions dominating over the PA_{Tc}+OH reactions, with R4>R2>R1>R3.

Table 3. Rate coefficients in molec cm^3 s^{-1} for reactions R1 - R8 calculated at T=200K, 250K, 298K and 350K. The first entry is the k_i, the second $p_i k_i$ and the third is the tunneling coefficient. The final column is the weighted sum $\sum_{i=1}^{8} p_i k_i$, i.e. k_{eff}.

$T(K)$	k_1	k_2	k_3	k_4
200	2.47x10^{-16} **2.46x10^{-16}** (7.12)	1.53x10^{-15} **3.12x10^{-18}** (7.29)	4.92x10^{-18} **4.91x10^{-18}** (1102.60)	1.61x10^{-13} **3.28x10^{-16}** (147.40)
250	9.34x10^{-16} **9.27x10^{-16}** (3.19)	4.25x10^{-15} **3.39x10^{-17}** (3.37)	1.42x10^{-17} **1.41x10^{-17}** (101.66)	7.08x10^{-14} **5.65x10^{-16}** (26.47)
298	2.64x10^{-15} **2.59x10^{-15}** (2.18)	9.64x10^{-15} **1.85x10^{-16}** (2.30)	3.60x10^{-16} **3.53x10^{-17}** (27.08)	5.09x10^{-14} **9.78x10^{-16}** (10.40)

350	6.57 x10^{-15} **6.33x10^{-15}** (1.73)	2.00x10^{-14} **7.56x10^{-16}** (1.81)	8.83x10^{-17} **8.50x10^{-17}** (11.13)	4.48x10^{-16} **1.69x10^{-15}** (5.57)	

$T(K)$	k_5	k_6	k_7	k_8	$\sum_{i=1}^{8} p_i k_i$
200	1.07x10^{-20} **1.07x10^{-20}** (5.91)	1.36x10^{-22} **2.78x10^{-25}** (12.56)	1.88x10^{-19} **1.87x10^{-19}** (4.64)	2.99x10^{-17} **6.10x10^{-20}** (4.93)	**5.83x10^{-16}**
250	1.59x10^{-19} **1.58x10^{-19}** (2.87)	4.94x10^{-21} **3.94x10^{-23}** (4.69)	1.61x10^{-18} **1.60x10^{-18}** (2.50)	8.45x10^{-17} **6.75x10^{-19}** (2.60)	**1.54x10^{-15}**
298	1.06x10^{-18} **1.04x10^{-18}** (2.02)	6.06 x10^{-20} **1.16x10^{-21}** (2.87)	7.36x10^{-18} **7.21x10^{-18}** (1.86)	1.88x10^{-16} **3.61x10^{-18}** (1.91)	**3.80x10^{-15}**
350	5.04x10^{-19} **4.85x10^{-18}** (1.64)	4.76x10^{-19} **1.79x10^{-20}** (2.10)	2.57x10^{-17} **2.48x10^{-17}** (1.54)	3.78x10^{-16} **1.42x10^{-17}** (1.57)	**8.90x10^{-15}**

The phenomenological rate coefficient k_{eff} must include the effect of the thermal weighting factors which strongly favors the PA_{Tc} conformer. The weighted partial rates, $p_i k_i$, for R1-R4 are plotted versus temperature in Fig. 8 along with the sum $k_{eff}=\Sigma p_i k_i$. It is seen that the influence of the acid hydrogen abstraction reaction R4 is greatly diminished by the Boltzmann averaging and the effective rate is now dominated the methyl abstraction reaction R1 except at temperatures below 225K. The effective rate coefficient has been fit to the generalized Arrhenius form

$k_{eff} = 1.50 \times 10^{-32}\ T^{6.75}\ e^{\frac{475.97}{T}}$ in units of molecule, cm^3, sec and K. Consequently, the predicted activation energy is positive. One recalls that the experimentally inferred PA_{Tc}/PA_{Tt} energetic splitting was 2.08 kcal/mol, or about 0.6 kcal/mol lower than our theoretical result. Even if the smaller experimentally inferred value is adopted, however, the apparent activation energy remains clearly positive although smaller by about 0.6 kcal/mol.

It is of interest to compare our theoretical calculation of $k_{eff}(T)$ to the experimental results $k_{obs}(T)$ of Mellouki and Mu.[23] A comparison of those results is plotted in Fig. 9. There are clearly some significant differences. The experimental results for k_{obs} are larger than theory by over an

order of magnitude and exhibit a negative activation energy. At 298K they report a rate constant of $1.2(\pm 0.4)\times 10^{-13}$ cm^3 s^{-1} that was inferred from the pseudo-first-order depletion rate of OH following HONO photolysis. The present theoretical results are instead closer to an older experimental value by Grosjean et al.[55] who reported a single estimated value of $< 5.0\times 10^{-14}$ cm^3 s^{-1} at 298K. It is interesting to note that the theoretical prediction for R4 alone lies much closer to the experiments of Mellouki and Mu. As illustrated in the figure, k_4 and k_{obs} are close in magnitude and show a similar negative activation energy. The R4 reaction is greatly de-emphasized in the full simulation due to the low thermal weighting of the PA_{Tt} conformer.

It is also interesting to compare with previous studies of an analog system, the OH+acetic acid (i.e. AA+OH) reaction.[56] [57] The AA molecule is structurally similar to PA, and exhibits abstraction reactions with OH from both the methyl and acid sites. However, since AA does not possess the ketone group there is no direct analog of the internally hydrogen bonded Tc conformer that dominates the PA distribution. Instead the AA reaction is most similar to $OH+PA_{Tt}$. As shown in Fig. , the rate coefficient for OH+AA shows a negative activation energy similar to the experimental results for PA+OH, and detailed modeling of AA reveals the mechanism is dominated by the acid site abstraction. It is tempting to speculate that for some reason the PA_{Tt} reagent conformer may have an enhanced contribution in the experiment, as is apparently the case in the condensed phase.

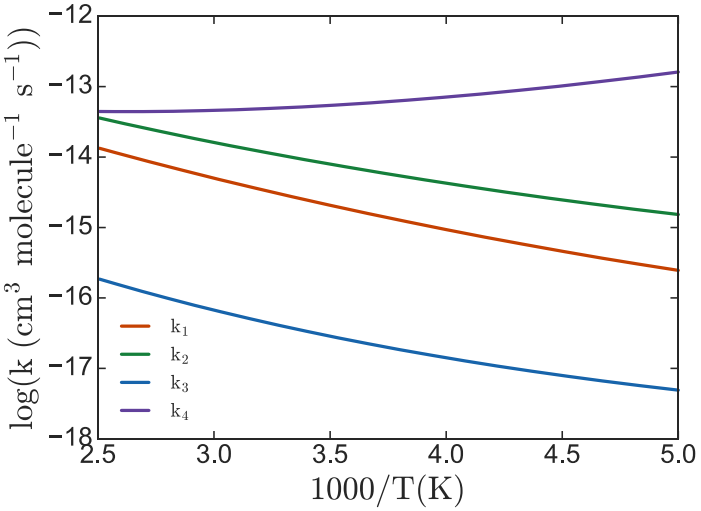

Figure 7. *The elementary rate coefficients for reactions of PA_{Tc}+OH (R1 and R3) and PA_{Tt}+OH (R2 and R4) obtained using eq. (4.1) with SCT tunneling. The rates are not thermally weighted in this figure.*

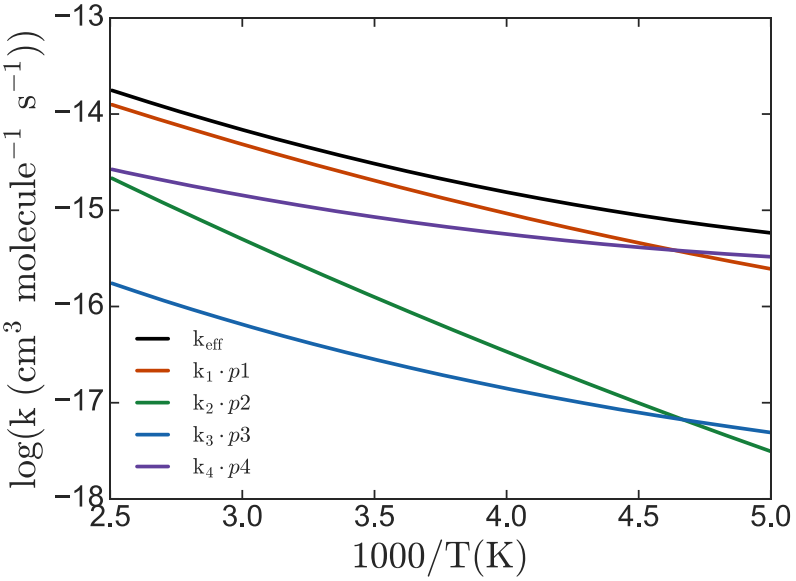

Figure 8. *Thermally weighted rate constants of PA+OH at the CCSD(T)/CBS level of theory as well as the effective rate constant $k_{eff}=\Sigma p_i k_i$.*

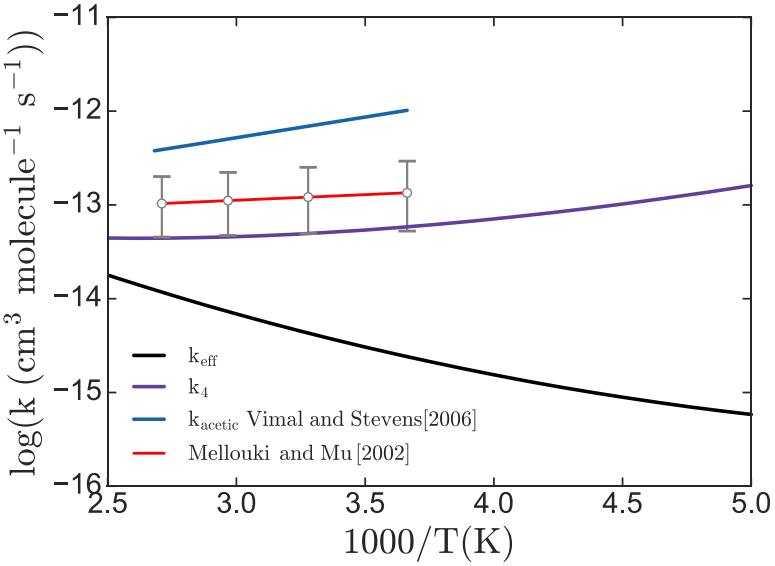

Figure 9. *The PA+OH rate coefficient $k_{eff}=\Sigma p_i k_i$.and k_4 computed for 200-400K along with the experimental values of Mellouki and Mu.*[23] *Also shown is the fit to experimental results for acetic acid+OH.*[56]

V. Conclusions

The rate coefficients for the reactions of OH with pyruvic acid were calculated using *ab initio* TST including quantum tunneling. We identified four reaction classes, two chemically distinct H-atom abstraction reactions, at the methyl and acid sites, and two distinct OH-addition reactions. The two reagent conformers, Tc and Tt, were found to exhibit very different chemical behavior. The Tc conformer was shown to favor methyl abstraction while the Tt conformer favored the acid site abstraction. Previous work has shown[34 58] that in carboxylic acids the acidic H atom is preferentially abstracted by OH in spite of the higher energy of the O-H compared with the C-H bond.[59] The present study finds that tunneling significantly modifies the PA rates at room temperature, especially for the acidic H atom abstraction reaction.

The addition reactions were found to be only of minor importance in the overall rate. The formation and interconversion of pre-reactive complexes, including roaming and conformational isomerization, was found not to significantly modify the rates since the backward rates, i.e. $\mathbf{k}_{-f}$, were significantly larger than the reactive rates, i.e $\mathbf{k}_r$. However, a kinetic theory that incorporates these effects was developed which may be applicable to other more suitable problems.

Comparison of the computed rate coefficients to the experiments of Mellouki and Mu[23] gave somewhat puzzling results. While experimental results agreed with the theoretical rate computed for PA_{Tt}+OH, it was in substantial disagreement with the predictions based on a thermal distribution of PA_{Tc} and PA_{Tt}. The experimental results exhibited a clear negative activation energy while the theory (statistically dominated by PA_{Tc}) showed a slower reaction with a positive activation energy. One might posit either experimental and theoretical sources for the discrepancy. It is conceivable that the experiment may have misestimated the actual gas phase concentration of PA present in the chamber. Pyruvic acid is a highly oxidized molecule which has a tendency to adsorb on the walls of reaction chambers.[60] This may result in the actual concentrations in the gas phase being different from the estimates used to compute k_{obs}. In principle the actual concentration could be directly measured using an FTIR probe.[61] Because of its high reactivity, OH radical loss to byproducts or walls is another potential source of error in the experimental rate constant.[62] Contaminants such as water and acidic acid recorded in the experiment[23] are able to hydrogen bond with PA and weaken the intramolecular hydrogen bond of the PA_{Tc} conformer changing the relative abundances of PA_{Tc}/PA_{Tt} . On the theoretical side, errors in the quantum chemistry are

potential source of error. We find that bringing down the TS barrier by about 2 kcal/mol for the OH+PA_{Tc} abstraction reaction would bring theory into agreement with experiment. We are also cognizant of the relatively high level of uncertainty of the barrier to OH-insertion. We note that the addition reaction barriers showed large differences between the M11 and CCSD(T) levels of theory. Further calculations may be warranted. Dynamically, it is possible that the tunneling coefficient has been underestimated. While the small curvature method is generally accurate, PA+OH is a heavy-light-heavy type reaction for which it may underestimate the tunneling effect. We also speculate that there might be a process operating we have not considered that accentuates the role of PA_{Tt} conformer in the reaction, which, as we noted, reacts at a rate similar to that observed in experiment. We note that a careful analysis of the reaction products may be revealing since the methyl site abstraction, favored by Tc, yields different nascent products than does acid site abstraction, favored by Tt.

Finally, we note in the context of atmospheric processing of pyruvic acid molecules, the present results seem to confirm the conclusion of Reed-Harris *et al* [18 20] that sunlight induced photolysis is the dominate loss channel. Indeed, under the conditions provided by normal tropospheric temperatures and pressures the rate coefficient of OH+PA is two orders of magnitude smaller than the photolysis rate, even if the PA is assumed to be entirely in the Tt state.

Acknowledgements

This work was supported by the National Science Foundation through grant CHE1556041. VV acknowledges support by the National Science Foundation (CHE 1611107), This work utilized the RMACC Summit supercomputer, which is supported by the National Science Foundation (awards ACI-1532235 and ACI-1532236), the University of Colorado Boulder, and Colorado State University. The Summit supercomputer is a joint effort of the University of Colorado Boulder and Colorado State University.

Supporting Information

The Supporting Information is available free of charge at https://pubs.acs.org/doi/xxxxxx.

- Energetic structural, and frequency parameters obtained for the stationary point computions from DFT and CCDS(T) calculations.
- The product structures for reactions R1-R8 displayed as a figure.

- A mathematical appendix presenting a microcanonical formulation of the multiconformational kinetic model presented in canonical form in Sec. 3 of the paper.

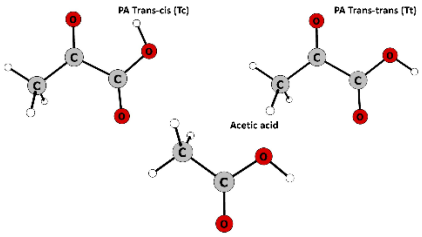

Table of Content Graphic

References:

[1] Atkinson, R.; Baulch, D. L.; Cox, R. A.; Hampson Jr, R. F.; Kerr, J. A.; Rossi, M. J.; Troe, J. Evaluated Kinetic, Photochemical and Heterogeneous Data for Atmospheric Chemistry: Supplement V. IUPAC Subcommittee on Gas Kinetic Data Evaluation for Atmospheric Chemistry. *J. Phys. Chem. Ref. Data* **1997**, *26* (3), 521–1011.

[2] W.B. DeMore, S.P. Sander, D.M. Golden, R.F. Hampson, M.J. Kurylo, C.J. Howard, A.R. Ravishankara, C.E. Kolb, and M.J. Molina, "Chemical Kinetics and Photochemical Data for Use in Stratospheric Modeling. Evaluation Number 12", JPL Publication 97-4, Jet Propulsion Laboratory, Pasadena, **1997**

[3] Truhlar, D. G., Garrett, B. C., & Klippenstein, S. J. (1996). Current status of transition-state theory. *J. Phys. Chem*., *100*, 12771-12800.

[4] Nguyen, T. B.; Bateman, A. P.; Bones, D. L.; Nizkorodov, S. A.; Laskin, J.; Laskin, A. High-Resolution Mass Spectrometry Analysis of Secondary Organic Aerosol Generated by Ozonolysis of Isoprene. *Atmos. Environ.* **2010**, *44* (8), 1032–1042.

[5] Carlton, A. G.; Turpin, B. J.; Lim, H.-J.; Altieri, K. E.; Seitzinger, S. Link between Isoprene and Secondary Organic Aerosol (SOA): Pyruvic Acid Oxidation Yields Low Volatility Organic Acids in Clouds. *Geophys. Res. Lett.* **2006**, *33* (6).

[6] Chebbi, A.; Carlier, P. Carboxylic Acids in the Troposphere, Occurrence, Sources, and Sinks: A Review. *Atmos. Environ.* **1996**, *30* (24), 4233–4249.

[7] Veres, P.; Roberts, J. M.; Burling, I. R.; Warneke, C.; de Gouw, J.; Yokelson, R. J. Measurements of Gas-phase Inorganic and Organic Acids from Biomass Fires by Negative-ion Proton-transfer Chemical-ionization Mass Spectrometry. *J. Geophys. Res. Atmos.* **2010**, *115* (D23).

[8] Andreae, M. O.; Talbot, R. W.; Li, S.-M. Atmospheric Measurements of Pyruvic and Formic Acid. *J. Geophys. Res. Atmos.* **1987**, *92* (D6), 6635–6641.

[9] Talbot, R. W.; Mosher, B. W.; Heikes, B. G.; Jacob, D. J.; Munger, J. W.; Daube, B. C.; Keene, W. C.; Maben, J. R.; Artz, R. S. Carboxylic Acids in the Rural Continental Atmosphere over the Eastern United States during the Shenandoah Cloud and Photochemistry Experiment. *J. Geophys. Res. Atmos.* **1995**, *100* (D5), 9335–9343.

[10] Grosjean, D.; Williams, E. L.; Grosjean, E. Atmospheric Chemistry of Isoprene and of Its Carbonyl Products. *Environ. Sci. Technol.* **1993**, *27* (5), 830–840.

[11] Bardouki, H.; Liakakou, H.; Economou, C.; Sciare, J.; Smolık, J.; Ždímal, V.; Eleftheriadis, K.; Lazaridis, M.; Dye, C.; Mihalopoulos, N. Chemical Composition of Size-Resolved Atmospheric Aerosols in the Eastern Mediterranean during Summer and Winter. *Atmos. Environ.* **2003**, *37* (2), 195–208.

[12] Bao, L.; Matsumoto, M.; Kubota, T.; Sekiguchi, K.; Wang, Q.; Sakamoto, K. Gas/Particle Partitioning of Low-Molecular-Weight Dicarboxylic Acids at a Suburban Site in Saitama, Japan. *Atmos. Environ.* **2012**, *47*, 546–553.

[13] Ho, K. F.; Lee, S. C.; Cao, J. J.; Kawamura, K.; Watanabe, T.; Cheng, Y.; Chow, J. C. Dicarboxylic Acids, Ketocarboxylic Acids and Dicarbonyls in the Urban Roadside Area of Hong Kong. *Atmos. Environ.* **2006**, *40* (17), 3030–3040.

[14] Baboukas, E. D.; Kanakidou, M.; Mihalopoulos, N. Carboxylic Acids in Gas and Particulate Phase above the Atlantic Ocean. *J. Geophys. Res. Atmos.* **2000**, *105* (D11), 14459–14471.

[15] Khwaja, H. A. Atmospheric Concentrations of Carboxylic Acids and Related Compounds at a Semiurban Site. *Atmos. Environ.* **1995**, *29* (1), 127–139.

[16] Limbeck, A.; Puxbaum, H.; Otter, L.; Scholes, M. C. Semivolatile Behavior of Dicarboxylic Acids and Other Polar Organic Species at a Rural Background Site (Nylsvley, RSA). *Atmos. Environ.* **2001**, *35* (10), 1853–1862.

[17] Kawamura, K.; Tachibana, E.; Okuzawa, K.; Aggarwal, S. G.; Kanaya, Y.; Wang, Z. F. High Abundances of Water-Soluble Dicarboxylic Acids, Ketocarboxylic Acids and α-Dicarbonyls in the Mountaintop Aerosols over the North China Plain during Wheat Burning Season. *Atmospheric Chem. Phys.* **2013**, *13* (16), 8285–8302.

[18] Reed Harris, A. E.; Doussin, J.-F.; Carpenter, B. K.; Vaida, V. Gas-Phase Photolysis of Pyruvic Acid: The Effect of Pressure on Reaction Rates and Products. *J. Phys. Chem. A* **2016**, *120* (51), 10123–10133.

[19] Reed Harris, A. E.; Cazaunau, M.; Gratien, A.; Pangui, E.; Doussin, J.-F.; Vaida, V. Atmospheric Simulation Chamber Studies of the Gas-Phase Photolysis of Pyruvic Acid. *The J. Phys. Chem. A* **2017**, *121* (44), 8348–8358.

[20] Reed Harris, A. E.; Pajunoja, A.; Cazaunau, M.; Gratien, A.; Pangui, E.; Monod, A.; Griffith, E. C.; Virtanen, A.; Doussin, J.-F.; Vaida, V. Multiphase Photochemistry of Pyruvic Acid under Atmospheric Conditions. *J. Phys. Chem. A* **2017**, *121* (18), 3327–3339.

[21] Rapf, R. J.; Vaida, V. Sunlight as an Energetic Driver in the Synthesis of Molecules Necessary for Life. *Phys. Chem. Chem. Phys* **2016**, *18* (30), 20067–20084.

[22] Reed Harris, A. E.; Ervens, B.; Shoemaker, R. K.; Kroll, J. A.; Rapf, R. J.; Griffith, E. C.; Monod, A.; Vaida, V. Photochemical Kinetics of Pyruvic Acid in Aqueous Solution. *J. Phys. Chem. A* **2014**, *118* (37), 8505–8516.

[23] Mellouki, A.; Mu, Y. On the Atmospheric Degradation of Pyruvic Acid in the Gas Phase. *J. Photochem. Photobio. A: Chem.* **2003**, *157*, 295–300.

[24] Klippenstein, S. J.; Cavallotti, C. Ab Initio Kinetics for Pyrolysis and Combustion Systems. In *Computer Aided Chemical Engineering*; Elsevier, **2019**; Vol. 45, pp 115–167.

[25]Takahashi, K.; Plath, K. L.; Skodje, R. T.; Vaida, V. Dynamics of Vibrational Overtone Excited Pyruvic Acid in the Gas Phase: Line Broadening Through Hydrogen-Atom Chattering, *J. Phys. Chem. A* **2008**, 112, 7321-7331.

[26] Plath, K. L.; Takahashi, K.; Skodje, R. T.; Vaida, V. Fundamental and Overtone Vibrational Spectra of Gas-Phase Pyruvic Acid, *J. Phys. Chem. A* **2009**, 113, 7294-7303.

[27] Seeman, J. I. Effect of Conformational Change on Reactivity in Organic Chemistry. Evaluations, Applications, and Extensions of Curtin-Hammett/Winstein-Holness Kinetics, *Chem. Rev.* **1983**, 83, 83-134.

[28] Vereecken, L.; Peeters, J. The 1,5-H-Shift in 1-Butoxy: A Case Study in the Rigorous Implementation of Transition State Theory for a Multirotamer System. *J. Chem. Phys.* **2003**, 119, 5159−5170.

[29] Zheng, J.; Meana-Pañeda, R.; Truhlar, D. G. MSTor version 2013: A New Version of the Computer Code for the Multi-Structural Torsional Anharmonicity, Now With a Coupled Torsional Potential, *Comput. Phys. Commun*. **2013**, 184, 2032−2033.

[30] Klippenstein, S. J.; Pande, V. S.; Truhlar, D. G. Chemical Kinetics and Mechanisms of Complex Systems: A Perspective on Recent Theoretical Advances, *J. Am. Chem. Soc.* **2014**, 136, 528−546.

[31] Smith, I. W.; Ravishankara, A. R. Role of Hydrogen-Bonded Intermediates in the Bimolecular Reactions of the Hydroxyl Radical, *J. Phys. Chem. A* **2002**, *106* (19), 4798–4807.

[32] Alvarez-Idaboy, J. R.; Mora-Diez, N.; Vivier-Bunge, A. A Quantum Chemical and Classical Transition State Theory Explanation of Negative Activation Energies in OH Addition to Substituted Ethenes. *J. Am. Chem. Soc.* **2000**, 122, 3715−3720.

[33] Alvarez-Idaboy, J. R.; Mora-Diez, N.; Boyd, R. J.; Vivier-Bunge, A. On the Importance of Prereactive Complexes in Molecule-Radical Reactions: Hydrogen Abstraction from Aldehydes by OH, J. *Am. Chem. Soc.* **2001**, 123, 2018−2024.

[34] Hansen, J. C.; Francisco, J. S. Radical-Molecule Complexes: Changing Our Perspective on the Molecular Mechanisms of Radical-Molecule Reactions and Their Impact on Atmospheric Chemistry. *ChemPhysChem* **2002**, 3, 833−840.

[35] Singleton, D. L.; Cvetanovic, R. J. Temperature-Dependence of Reactions of Oxygen-Atoms with Olefins. *J. Am. Chem. Soc*. **1976**, 98, 6812−6819.

[36] Kaufman, F. Kinetics of Elementary Radical Reactions in the Gas Phase, *J. Phys. Chem.* **1984**, 88, 4909-4917.

[37] Patrick, R.; Barker, J. R.; Golden, D. M. Computational Study of the HO_2+HO_2 and DO_2+DO_2 Reactions, *J. Phys. Chem.* **1984**, 88, 128-136.

[38] Georgievskii, Y.; Klippenstein, S. J. Strange Kinetics of the C_2H_6+CN Reaction Explained, *J. Phys. Chem. A* **2007**, 111, 3802-3811.

[39] Chen, Y.; Rauk, A.; Tschuikow-Roux, On the Question of Negative Activation Energies: Absolute Rate Constants by RRKM, *J. Phys. Chem*. **1991** 95, 9900-9908.

[40] Zhou, D.D.Y.; Han, K. L.; Zhang, P. Y.; Harding, L. B.; Davis, M. J.; Skodje, R. T. Theoretical Determination of the Rate Coefficient for the $HO_2+HO_2 \rightarrow H_2O_2+O_2$ Reaction: Adiabatic Treatment of Anharmonic Torsional Effects, *J. Phys. Chem. A* **2012***,* 116, 2089-2100.

[41] Hermans, I.; Jacobs, P.; Peeters, J. Pronounced Non-Arrhenius Behaviour of Hydrogen-Abstractions from Toluene and Derivatives by Phthalimide-N-oxyl Radicals: A Theoretical Study. *Phys. Chem. Chem. Phys.* **2008**, 10, 1125−1132.

[42] Mozurkewich, M.; Benson, S. W. Negative Activation Energies and Curved Arrhenius Plots. 1. Theory of Reactions over Potential Wells, *J. Phys. Chem.* **1984**, 88, 6329-6435.

[43] Skodje, R. T.; Truhlar, D. G.; Garrett, B. C. A General Small Curvature Approximation for Transition-State-Theory Transmission Coefficients, *J. Phys. Chem.* **1981**, 85, 3019-3023.

[44] Liu, Y. P.; Lynch, G. C.; Truong, T. N.; Lu, D. H.; Truhlar, D. G.; Garrett, B. C. Molecular Modeling of the Kinetic Isotope Effect for the [1,5]-Sigmatropic Rearrangement of Cis-1,3-Pentadiene. *J. Am. Chem. Soc.* **1993**, *115*, 2408–2415.

[45] Peverati, R.; Truhlar, D. G. Improving the Accuracy of Hybrid Meta-GGA Density Functionals by Range Separation, *J. Phys. Chem. Lett.* **2011**, 2, 2810-2817.

[46] Church, J.R.; Skodje, R.T."Double Hydrogen-Atom Exchange Reactions of HX(X=F, Cl, Br, I) with HO_2", *J. Phys. Chem. A* **2018**, 122, 5251-5260.

[47] Schmidt, M. W.; Baldridge, K. K.; Boatz, J. A.; Elbert, S. T.; Gordon, M. S.; Jensen, J. H.; Koseki, S.; Matsunaga, N.; Nguyen, K. A.; Su, S. General atomic and molecular electronic structure system *J. Comput. Chem.* **1993**, 14, 1347– 1363.

[48] The 0.967 value was an estimate of the scaling factor for the Minnesota family of functionals based on a compromise of zero-point and excitation (fundamental) considerations http://cccbdb.nist.gov/vibnotes.asp, http://comp.chem.umn.edu/freqscale/version3b1.htm.

[49] Gonzalez, C.; Schlegel, H. B. Reaction Path Following in Mass-Weighted Internal Coordinates. *J. Phys. Chem.* **1990**, *94* (14), 5523–5527.

[50] Gaussian 16, Revision B.01, M. J. Frisch, et al. Gaussian, Inc., Wallingford CT, **2016**.

[51] Reva, I. D.; Stepanian, S. G.; Adamowicz, L.; Fausto, R. Combined FTIR Matrix Isolation and Ab Initio Studies of Pyruvic Acid: Proof for Existence of the Second Conformer. *J. Phys. Chem. A* **2001**, *105* (19), 4773–4780.

[52] Schellenberger, A.; Beer, W.; Oehme, G. Untersuchungen zur theorie der α-ketosäuren—XI. IR-spektroskopische untersuchungen an α-ketosäuren im gaszustand. *Spectrochimica Acta* **1965**, *21* (7), 1345–1351.

[53] Bao, J. L.; Truhlar, D. G. Manual for SS-QRRK Utility Code. SS-QRRK: A Program for System-Specific Quantum Rice-Ramsperger-Kassel Theory. POLYRATE Version 2016-2A. *University of Minnesota: Minneapolis, MN* **2017**.

[54] Barker, J. R. Multiple-Well, Multiple-path Unimolecular Reaction Systems. I. MultiWell Computer Program Suite. *Int. J. Chem. Kinet.* **2001**, *33*, 232–245.

[55] Grosjean, D. Atmospheric Reactions of Pyruvic Acid. *Atmos. Environ.* **1983**, *17* (11), 2379–2382.

[56] Vimal, D.; Stevens, P. S. Experimental and Theoretical Studies of the Kinetics of the Reactions of OH Radicals with Acetic Acid, Acetic Acid-d3 and Acetic Acid-d4 at Low Pressure, *J. Phys. Chem. A* **2006**, 110, 11509-11516.

[57] Rosado-Reyes, C. M.; Francisco, J. S. *J. Phys. Chem. A* **2006**, 110, 4419.

[58] Sun, W.; Yang, L.; Yu, L.; Saeys, M. Ab Initio Reaction Path Analysis for the Initial Hydrogen Abstraction from Organic Acids by Hydroxyl Radicals. *J. Phys. Chem. A* **2009**, *113* (27), 7852–7860.

[59] Blanksby, S. J.; Ellison, G. B. Bond Dissociation Energies of Organic Molecules. *Acc. Chem. Res* **2003**, *36* (4), 255–263.

[60] Harris, A. R. A Kinetic and Mechanistic Study of the Photochemistry of Pyruvic Acid: Implications for the Atmosphere, PhD thesis, University of Colorado **2017**.

[61] Plath, K. L.; Takahashi, K.; Skodje, R. T.; Vaida, V. Fundamental and Overtone Vibrational Spectra of Gas-Phase Pyruvic Acid. *J. Phys. Chem. A* **2009**, *113* (26), 7294–7303.

[62] Faloona, I. C.; Tan, D.; Lesher, R. L.; Hazen, N. L.; Frame, C. L.; Simpas, J. B.; Harder, H.; Martinez, M.; Di Carlo, P.; Ren, X. A Laser-Induced Fluorescence Instrument for Detecting Tropospheric OH and HO2: Characteristics and Calibration. *J. Atmos. Chem.* **2004**, *47* (2), 139–167.